A Framework to Create Realistic IVUS Phantoms for Different Intraluminal Pressures

Fernando Mitsuyama Cardoso, Matheus Cardoso Moraes, Sérgio Shiguemi Furuie

University of São Paulo, Brazil

Abstract

Intravascular Ultrasound (IVUS) phantoms allow flexibility and full vessel and atherosclerotic-parameter control. Controlling coronary properties in phantoms is important to calibrate and test many different IVUS algorithm. Therefore, a framework to create representative IVUS phantoms, using Finite Element method and Field II, is presented. First, a coronary cross section model is selected. Second, the different regions of an IVUS image are assigned for the elasticity modulus. Third, triangular element is used to automatically generate the IVUS mesh, higher number of elements are disposed at borders, where more precision is required. Finally, the deformation is computed, using different intraluminal pressure. Consequently, the deformed image is generated, and Field II is applied to incorporate the Speckle noise. The framework is corroborated by creating phantoms with different features, and comparing the plaque strain rate, with deformations obtained by recent studies. Moreover, related modalities, such as Intravascular OCT and MRI can be included in this framework for future investigations.

1. Introduction

Atherosclerosis rupture initiates 75% of acute myocardial infarction [1]. Intravascular Elastography is an imaging technique, which an elasticity map is created by associating images at the same region acquired in different intraluminal pressures. Hence, composition, and vulnerability can be detected based on their different mechanical properties. Therefore, it comes to be very useful for coronary disease diagnoses [2]. An intravascular Ultrasound (IVUS) phantom is a very useful algorithm performance optimization and validation tool, where investigators can have high degree of freedom to control the pertinent parameters [2, 3]. Specifically in [2, 4, 5], polyvinyl alcohol cryogel phantoms are used. Computational phantoms are found in [6, 7, 8], where Finite Element is applied to create IVUS phantoms with different intraluminal pressure, the phantoms are used to evaluate and discuss some coronary and plaques mechanical properties. As can be seen from the literature, there is no reasonable number of algorithms, directly devoted to create realistic computational IVUS phantoms. Therefore, a framework mainly devoted to the creation of phantoms, comes to be of great help for IVUS image investigator.

2. Materials and methods

The current framework involved creating and corroborating realistic IVUS phantoms. A desktop computer with an Intel Core 2 Duo 2.53 GHz, 4 GB of RAM, a Windows Vista 32 bits and MATLAB (2009a) with Imaging Processing and Partial Differential Equation Toolbox were used. The evaluation was performed by comparing the deformations, with prior studies.

The methodology is based on combining Finite Element method and Field II to create realistic IVUS phantoms. The entire process is divided in three steps. The **Model Selection**, where different coronary cross-section model (Mi) (Figure 1(a)) can be chosen, and Field II is applied to incorporate speckle; hence, generating the scatterer map (S_{Map}), (Figure 1(c)). In the **Numerical Modeling** block, the borders, are identified to serve as positions for the primary nodes. Thus, Delaunay triangulation is carried out for the mesh (Msh) construction [9]. The lumen and external border of an IVUS are used for the intraluminal forces and boundary conditions, respectively. Consequently, the intraluminal pressure and Young Modulus are applied, and the deformation is computed by FEM, generating the deformed mesh ($Msh_{Deformed}$) (Figure 1(b)). Finally, the **Matching** block associates the $Msh_{Deformed}$ with S_{Map} to create the deformed scatterer map (DS_{Map}) (Figure 1(d)).

2.1. Model selection

A number of coronary cross section templates in a diastole cardiac phase, with different atherosclerotic plaques was generated (Mi) (Figures 3(a), (b) and (c)).
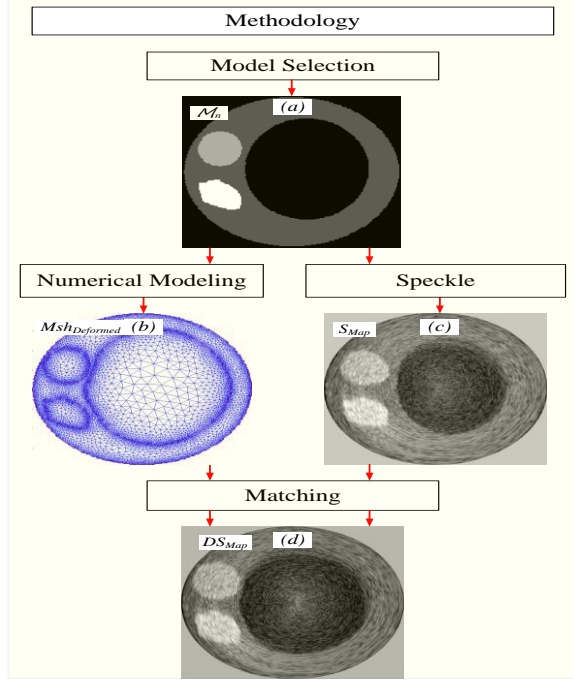
Figure 1: Block diagram of the Methodology.

The scatterer distribution is performed by Field II [10]; thus, generating the noisy image S_{Map} (Figure 1(c)). The parameters used were 256 arrays of transducers, with frequency set to $40MHz$ and 200.000 scatterers.

2.2. Numerical modeling

Finite element (FEM) [6, 7, 8, 9, 11, 12] is used to create representative coronary artery systems and their corresponding deformation. Two sub-blocks, summarizes the FEM process, **Mesh Generation**, and **Strain Estimation**.

Mesh Generation - The mesh is a number of geometric shape elements, representing the regions of a coronary [9]. As the regions have different elastic properties, the borders will provide important mechanical information. Therefore, to have a maximized precision, the first set of nodes might be placed at borders. Consequently, first, the Laplacian is computed:

$$I_{borders} = \Delta M_n, \tag{1}$$

where, Δ is the Laplacian operator, M_n is the chosen model (Figure 1(a)), and $I_{borders}$ are the borders of M_n. Hence, the positions for the first set of nodes can be found by:

$$P_{Nodes}^{FirstSet} = p\left(I_{border}\right), \tag{2}$$

where, $p\left(I_{border}\right)$ are the border positions, The mesh matrix, *Msh* is completed using Delaunay triangulation:

$$Msh = \begin{bmatrix} \tau_e & P_i & P_j & P_m & R \end{bmatrix}, \tag{3}$$

where, τ_e is any triangular element, P_i, P_j and P_m are the corresponding node position of the element, τ_e (Figure 2(a)), and *R* is the region, where the element belongs. The triangular element was used, by being the simplest finite element shape [9], minimizing computational cost. In addition, an acceptable triangular shape, in which the vertex angle ranges between $15^o - 165^o$ [9], is assured by Delaunay triangulation.

Strain Estimation - Strain is a process of changing the shape of a body according to the force applied, and the body parameters [11, 9]. The parameters concerning the arterial system are defined based on mechanical, physiological, and anatomical coronary aspects.

The nodal force vector (*F*) is applied perpendicularly to the lumen border, it can be represented by two sources, the intraluminal arterial pressure, the difference between systole and diastole (PA =120-80 = 40mmHg), and the pressure produced by an inflated balloon (2atm = 1520mmHg, for instance) [2, 6, 7, 8].

The global stiffness matrix (*K*), is obtained by the vessel mechanical properties, Poisson ratio (*v*=0.5) and Young modulus (E = 600kPa, 80kPa, 5000kPa, 600kPa, 296kPa, and 25kPa, for media, adventitia, and calcified, fibrous, fibro-lipidic, and highly lipidic, respectively) [6, 7, 8, 13, 14].

The boundary conditions are defined to be the outermost nodes position. Therefore, by assigning the pertinent parameter values, boundary conditions, and applying the force using FEM, the deformed mesh is generated $Msh_{Deformed}$. (Figure 1(b)).

2.3. Matching

Matching equivalent regions of deformed and non-deformed images is important to create realistic phantoms [7]. Therefore, the scatterer distribution matrix S_{Map} is associated to the mesh *Msh*; thus, the new deformed scatter distribution (DS_{Map}), corresponding to the deformed mesh $Msh_{Deformed}$ is accurately generated. The DS_{Map} is obtained by relating the position (*p*) of each scatterer from S_{Map} to the pertinent triangle of the *Msh* (Figure 2(a)).

$$p = c_i P_i + c_j P_j + c_m P_m, \tag{4}$$

where, c_i, c_j, and c_m are the proportional distance from *p* to the element nodes, P_i, P_j, and P_m, respecting the following conditions:

$$\begin{aligned} c_i, c_j, c_m &\geq 0, \\ c_i, c_j, c_m &\leq 1, \\ c_i + c_j + c_m &= 1. \end{aligned} \tag{5}$$

Consequently, the linear system is constructed:

$$\{p\} = \left[P_{Nodes}^e \right]\{c\}, \tag{6}$$

where, p is the scatterer position, P^e_{Nodes} are the node positions, P_i, P_j, and P_m of the element, and c is the constant vector of the proportional distance; thus it can be written,

$$\begin{Bmatrix} x \\ y \\ 1 \end{Bmatrix} = \begin{bmatrix} x_i & x_i & x_m \\ y_i & y_j & y_m \\ 1 & 1 & 1 \end{bmatrix} \begin{Bmatrix} c_i \\ c_j \\ c_m \end{Bmatrix}, \quad (7)$$

where, "1" is set to the third line of the p and P^e_{Nodes}, to satisfy the condition (5). Hence, the c vector can be found. Since the proportion of the c vector does not change when the triangle is deformed, the new scatterer position (p') (Figure 2(b)), and consequently the DS_{Map}(Figure 1(d)), are found by relating the c vector with the new node positions, from the deformed mesh $Msh_{Deformed}$,

$$\{p'\} = \left[P'^e_{Nodes} \right] \{c\}, \quad (8)$$

where, P'^e_{Nodes}, are the nodes coordinates of the deformed triangular element from $Msh_{Deformed}$ (Figure 2(b)).
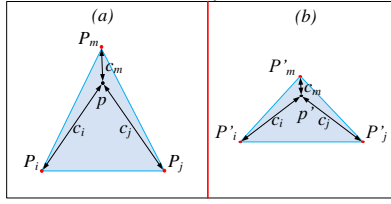

Figure 2: Overall view of the Matching method. (a) scatterer position in a triangular element. (b) New scatterer position in a deformed triangular element.

3. Results

The evaluation was performed by creating 3 phantoms and comparing the obtained deformation with related studies. The models have different atherosclerotic plaques, calcified, fibro-lipidic and highly lipidic, white, brown, and yellow, respectively (Figures 3(a), (b), and (c)) [6, 7, 8, 13]. The deformation was computed with the intraluminal pressure of an inflated balloon (2atm = 1520mmHg) [2], and the parameters mentioned in the Methodology. As can be seen in Figures 3(g), (h), and (i) the deformations are proportional to the stiffness of each type of tissue. In addition, as it was described in the Matching section, the DS_{Map} (Figures 3(j), (l), and (m)) were precisely reconstructed by associating S_{Map} (Figures 3(d), (e), and (f)) and the $Msh_{Deformed}$ (Figures 3(g), (h), and (i)).

The strain result was corroborated by computing and comparing the obtained strain of each plaque and comparing to pertinent studies. The strain rate can be obtained by:

$$\hat{\varepsilon} = \frac{\Delta_L}{Lo}, \quad (9)$$

where Lo is the plaque radial length from the Model, which is at diastole cardiac phase, Δ_L is the compression length after a given intraluminal pressure. As each plaque is homogeneous, a very close and simpler strain estimation can be obtained by the ratio of the plaque area variation, in two different intraluminal pressure:

$$\varepsilon = \frac{Area(Plaque_{High Pressure}) - Area(Plaque_{Low Pressure})}{Area(Plaque_{Low Pressure})}. \quad (10)$$

By estimating the strain of the three different plaques (Table 1), the framework is corroborated by having similar results to the prior studies [2, 6, 7, 8].
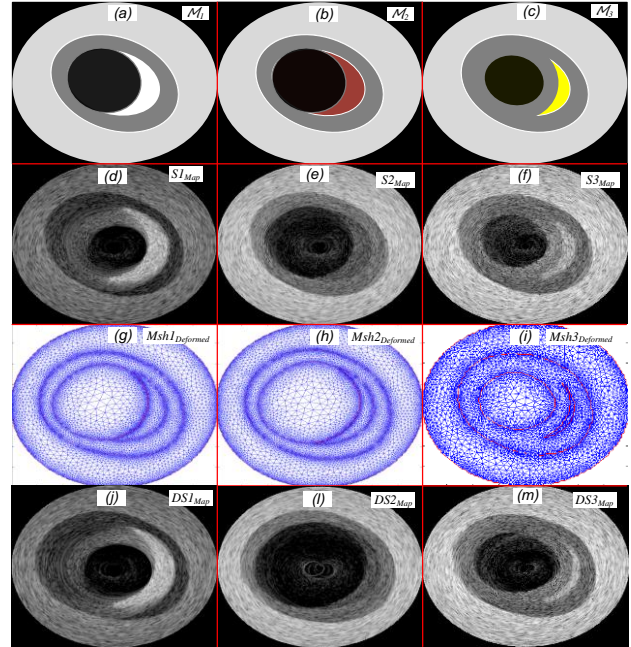

Figure 3: (a), (b) and (c) The models used as cross-section coronary artery with calcified fibro-lipidic and highly lipidic plaques, white, brown, and yellow, respectively. (d), (e) and (f) The corresponding S_{Map} images representing the IVUS phantoms in diastole. (g), (h) and (i) the corresponding deformed meshes. (j), (l) and (m) the corresponding final deformed images with Speckle incorporated.

4. Discussion and conclusion

Former studies have shown the importance of Elastography and phantoms for coronary disease investigators [2, 6, 7, 8]. As a result, many aspects of the coronary and atherosclerotic plaques are now solid. Nonetheless, as it was shown in the Introduction, this disease mortality is still a crucial issue. Therefore, alternative approaches are necessary.

The proposed framework shows how to create IVUS

phantoms with different features using different intraluminal pressure. The framework is corroborated visually (Figure 3), where the deformations are well correlated to the tissue stiffness, and also, by comparing the obtained result with outcomes from literature, which a 2atm inflated balloon was also applied. As can be seen from Table 1, in $M02$, the fibro-lipidic had a deformation close to -7%, the same obtained by [2] with in vivo analysis. The calcified plaque at $M01$, had a strain of +2.5%, the value and signal are very close to [6, 7], considering the different intraluminal pressure applied. In addition, as it has happened to other studies [6, 7] the calcified plaque presented an increase in its overall area. It is because the intraluminal pressure expands the vessel wall and the calcified plaque, as this plaque is hard it will not have a proportional compression in its width, since the entire plaque can move towards the vessel wall, which is much softer. Finally, in $M03$ the highly-lipidic tissue strain, 37%, is very close to the one obtained in [2], which was 40%, with in vivo studies.

Table 1. Strain rate of each model.

| Models | Type of Atherosclerotic Plaque | | |
	Highly-lipidic	Fibro-lipidic	Calcified
$M01$			+2.47%
$M02$		-6.70%	
$M03$	-37%		

In conclusion, a framework to create IVUS phantoms has been introduced, and its accuracy corroborated with recent studies, encouraging the evolution of the approach. The main contributions are: a) The way the mesh is constructed, where precision is maximized at borders; b) A matching method that estimates where the scatterer will be positioned after deformation. Simulation with a high precise echoic amplitudes and a widely combination of plaques and vessel features were not in the scope of this work. Therefore, future works will include these missing facts, as well as being adapt to related modality such as Intravascular OCT and MR.

Acknowledgements

References

[1] Danilouchkine MG, Mastik F, van der Steen AFW. Reconstructive Compounding for IVUS Palpography. IEEE Transaction on Ultrasonic Ferroelectric Frequency and Control 2009;56(12):2630-2642.

[2] de Korte CL, van der Steen AFW. Intravascular ultrasound elastography: an overview. Ultrasonics 2002;40:859–865.

[3] King DM, Moran CM, McNamara JD, Fagan AJ, Browne JE. Development of a vessel-mimicking material for use in anatomically realistic Doppler flow phantoms. Ultrasound in Medicine and Biology 2011;37(5):813-826.

[4] Liang Y, Zhu H, Friedman MH. Estimation of the transverse strain tensor in the arterial wall using ivus image registration. Ultrasound in Medicine and Biology 2008; 34(11):1832−1845.

[5] Nadkarni SK, Austin H, Mills G, Boughner D, Fenster A. A pulsating coronary vessel phantom for two and three-dimensional intravascular studies. Ultrasound in Medicine and Biology 2003;29(4):621-628.

[6] Le Floc'h S, Ohayon J, Tracqui P, Finet G, Gharib AM, Maurice RL, Cloutier G, Pettigrew RI. Vulnerable atherosclerotic plaque elasticity reconstruction based on a segmentation-driven optimization procedure using strain measurements: Theoretical framework. IEEE Transaction on Medical Imaging 2009; 28(7):1126–1137.

[7] Le Floc'h S, Cloutier G, Finet G, Tracqui P, Pettigrew RI, Ohayon J. On the potential of a new IVUS elasticity modulus imaging approach for detecting vulnerable atherosclerotic coronary plaques: in vitro vessel phantom study. Physics in Medicine and Biology 2010;55:5701-5721.

[8] Maurice RL, Cloutier G, Ohayon J, Finet G, Cloutier G. Adapting the lagrangian speckle model estimator for endovascular elastography: Theory and validation with simulated radio-frequency data. Journal of Acoustic Society of America 2004;116(2):1276−1286.

[9] Reddy JN. An Introduction to the Finite Element Method, 3rd Edition. New York: McGraw-Hill, 2006.

[10] Jensen JA, Svendsen NB. Calculation of pressure fields from arbitrarily shaped, apodized, and excited ultrasound transducers. IEEE Transaction on Ultrasonic Ferroelectric Frequency and Control.1992; 39:262–267.

[11] Zienkiewicz OC, Taylor RL, Zhu JZ. The Finite Element Method: Its Basis & Fundamentals, 6th Edition. Great Britain: Elsevier, 2010.

[12] Zienkiewicz OC, Taylor RL, Zhu JZ. The Finite Element Method: For Solid and Structural Mechanics, 6th Edition. Great Britain: Elsevier, 2010.

[13] de Korte CL, Céspedes EI, van der Steen AFW. Influence of catheter position on estimated strain in intravascular elastography. IEEE Trans Ultrason Ferroelec Freq Control 1999;46(3):616–625.

[14] Baldewsing RA, de Korte CL, Schaar JA, Mastik F, van der Steen AFW. A finite element model for performing intravascular ultrasound elastography of human atherosclerotic coronary arteries. Ultrasound Med Biol 2004;30(6):803–813.

Address for correspondence.
Name. Fernando Mitsuyama Cardoso
Full postal address. Laboratório de Engenharia Biomédica – Departamento de Telecomunicaçõe e Controle - Escola Politécnica da USP - Av. Prof. Luciano Gualberto, Travessa 3, 158 - sala D2-06 CEP 05508-970 São Paulo - SP - Brazil
E-mail address. Fernando.okara@gmail.com